Journal of Computational and Applied Mathematics 236 (2012) 4798–4809

Contents lists available at SciVerse ScienceDirect

Journal of Computational and Applied Mathematics

journal homepage: www.elsevier.com/locate/cam

Saltwater intrusion modeling: Verification and application to an agricultural coastal arid region in Oman

M. Walther [a,*], J.-O. Delfs [b], J. Grundmann [c], O. Kolditz [b,d], R. Liedl [a]

[a] Technische Universität Dresden, Institute for Groundwater Management, D-01062 Dresden, Germany

[b] Helmholtz-Centre for Environmental Research - UFZ, Department of Environmental Informatics, Permoserstr. 15, D-04318 Leipzig, Germany

[c] Technische Universität Dresden, Institute of Hydrology and Meteorology, D-01062 Dresden, Germany

[d] Technische Universität Dresden, Faculty of Forest-, Geo- and Hydro-Sciences, D-01062 Dresden, Germany

ARTICLE INFO

Article history:
Received 31 October 2011
Received in revised form 3 February 2012

Keywords:
Saltwater intrusion
Density-dependent
Three-dimensional numerical simulation
OpenGeoSys
Al-Batinah
IWAS-Oman

ABSTRACT

This paper deals with numerical modeling of density-dependent flow of saltwater intrusion in coastal groundwater systems. We present the implementation of an approach to solve a moving boundary problem for a dynamic water table within an invariant finite element mesh. The model is successfully validated against laboratory experiment data for an unconfined, density-dependent benchmark. The validated software is applied to a regional-scale study area and sufficiently calibrated for a steady state of pre-development conditions. Transient mass transport scenario simulations show good concordance with salinity measurements satisfyingly supporting the model setup.

1. Introduction

In many parts of the world, fresh water resources are getting scarcer and the access to potable water more and more limited for a growing number of people. When surface water supply is limited, groundwater exploitation and concurrent land surface subsidence [1] as well as saltwater intrusion are common problems in near-coastal areas, e.g. in North America [2], Mexico [3], or Australia [4]. To evaluate possible remediation scenarios, the challenges are usually assessed by the use of numerical models.

An overview on density-dependent flow gives [5], while further recent work includes [6–13] or [14] dealing with saltwater intrusion at locations all over the world. Before using numerical models as a tool for evaluation, it is crucial to validate these models against real-world data, using benchmarks like the "Henry problem", the "Elder problem", or upconing scenarios (compare [15]).

Desai [16], Desai and Li [17] suggested residual schemes to simulate groundwater flow on an invariant finite element mesh with a dynamic water table. For density-dependent flow (i.e. saltwater intrusion) see [18], where the residual flow vector is computed with conductivity as a function of hydraulic pressure above the water table and in the saltwater zone. Most alternative approaches to simulate unconfined transient groundwater flow are based on the boundary element method, e.g. [19,20], rely on the Dupuit–Forchheimer approximation, e.g. [21], or are mesh-free methods, e.g. [22].

* Corresponding author.
E-mail address: marc.walther@tu-dresden.de (M. Walther).

0377-0427/$ – see front matter
doi:10.1016/j.cam.2012.02.008

Symbols

A_i	area of isoline contours [m^2]
$\mathbf{D}$	dispersion tensor [$m^2\ s^{-1}$]
D_m	molecular diffusion coefficient [$m^2\ s^{-1}$]
$\mathbf{g}$	unit gravity vector [$m\ s^{-2}$]
h	hydraulic head [m]
h_f	hydraulic head of freshwater [m]
h_s	hydraulic head of saltwater [m]
$\mathbf{K}$	reduced hydraulic conductivity [$m\ s^{-1}$]
$\mathbf{k}$	reduced permeability tensor [m^2]
p	pressure [Pa]
p_{res}	residual pressure [Pa]
Q_{in}	boundary influx [$m^3\ s^{-1}$]
$Q_{\text{in,sub}}$	upstream subsurface inflow [$m^3\ s^{-1}$]
$Q_{\text{abstr,total}}$	abstraction rate [$m^3\ s^{-1}$]
Q_{total}	total estimated abstraction rate [$m^3\ s^{-1}$]
q_{spec}	specific abstraction rate [$m\ s^{-1}$]
q	source term [$m\ s^{-1}$]
q_ω	source term of mass transport [s^{-1}]
S_0	specific storativity [–]
t	time [s]
t_{final}	final time [s]
$\mathbf{v}$	fluid viscosity vector [$m\ s^{-1}$]
$v_{i,j}$	transverse or longitudinal components of velocity vector [$m\ s^{-1}$]
v	average fluid velocity [$m\ s^{-1}$]
z	elevation [m]
α_T	transverse dispersivity [m]
α_L	longitudinal dispersivity [m]
γ_ω	seawater–freshwater density relation coefficient [–]
Δt	time step [s]
Δx	element length in x-direction [m]
Δz	element length in z-direction [m]
$\boldsymbol{\delta}$	Kronecker-delta [–]
ζ	reduction factor [–]
ζ_{res}	residual value of reduction factor [–]
ζ_{eff}	effective reduction factor [–]
ζ_{smooth}	smoothed reduction factor [–]
ζ_p	pressure dependent reduction factor [–]
μ	fluid viscosity [Pa s]
ρ	density [$kg\ m^{-3}$]
ρ_0	reference density [$kg\ m^{-3}$]
ρ_f	density of freshwater [$kg\ m^{-3}$]
ρ_s	density of saltwater [$kg\ m^{-3}$]
ρ'	correlation coefficient [–]
σ	deviation [–]
τ	tortuosity [–]
ϕ	porosity [–]
ω	mass fraction [–].

The article at hand describes the application of a numerical groundwater model to a coastal region in Oman. This work includes an extension of the numerical simulation software OpenGeoSys (OGS, see Section 2) by a numerical scheme in [18] to simulate flow of multicomponents (e.g. fresh and saltwater) in unconfined aquifers. The numerical model is first validated against a laboratory saltwater intrusion experiment presented by Goswami and Clement [23]. Afterwards, we present the calibration of the heterogeneous regional-scale model and a scenario simulation of saltwater intrusion.

2. Governing equations

2.1. Simulation software package OpenGeoSys

For the simulation, the open source scientific modeling software OpenGeoSys (OGS) is used [24,25]. OGS is based on the Galerkin-FEM method and is able to model several thermo, hydro, mechanical and chemical processes (THMC) in porous and fractured media including the coupling among these processes. The implementation of the free-water table has been verified with the Dupuit–Forchheimer approximation. An unconfined density-dependent benchmark is shown in Section 3.

2.2. Basic equations for density-dependent flow

For this study case, the following conservation equation is used to describe subsurface water movement.

$$S_0 \frac{\partial h}{\partial t} - \nabla (\phi \mathbf{v}) = q \tag{1}$$

with the momentum balance equation for variable density flow in a porous medium using the Boussinesq approximation [26] as

$$\mathbf{v} = -\mathbf{K} (\nabla p + \rho \mathbf{g}) \tag{2}$$

where S_0 is specific storativity, h is hydraulic head, t is time, ϕ is porosity, $\mathbf{v}$ is fluid velocity vector, q is source term, p is pressure, ρ is density, $\mathbf{g}$ is unit gravity vector and $\mathbf{K}$ is reduced hydraulic conductivity tensor with

$$\mathbf{K} = \frac{\mathbf{k} \rho g}{\mu} \tag{3}$$

with $\mathbf{k}$ is reduced permeability tensor and μ dynamic viscosity. We define

$$\mathbf{k} = \zeta \mathbf{k_0} \tag{4}$$

where $\mathbf{k_0}$ is permeability tensor and ζ is a reduction factor following [18]:

$$\zeta = \begin{cases} \zeta_{\text{res}} & p \le p_{\text{res}} \\ \zeta_{\text{eff}} & p_{\text{res}} < p < 0 \\ 1 & p \ge 0 \end{cases} \tag{5}$$

where ζ_{res} is a given residual value for the reduction factor and $p_{\text{res}} < 0$ a given pressure, where ζ_{res} should be reached. This approach follows [18] and allows to determine the position of an a priori unknown groundwater table ("free groundwater table") of an unconfined aquifer. The method is based on a pressure-dependent reduction of hydraulic conductivity above the groundwater table. However, complete water saturation is maintained everywhere. In terms of calculation errors, p_{res} depends on the vertical grid resolution and should not be <-100 Pa especially for coarse meshes. $\zeta_{\text{res}} < 10^{-6}$ may lead to oscillations within the flow field, and $\zeta_{\text{res}} > 10^{-1}$ might cause water balance errors due to the low reduction. The effective reduction factor ζ_{eff} is defined as follows.

$$\zeta_{\text{eff}} = \zeta_{\text{res}} + (1 - \zeta_{\text{res}}) \zeta_{\text{smooth}} \tag{6}$$

with

$$\zeta_{\text{smooth}} = \zeta_p^{2(1-\zeta_p)} \tag{7}$$

and

$$\zeta_p = 1 - \frac{p}{p_{\text{res}}}. \tag{8}$$

Furthermore, mass transport is calculated by the advection–dispersion equation [27]

$$\phi \frac{\partial \omega}{\partial t} + \nabla \cdot (\phi \mathbf{v} \omega) - \nabla \cdot (\phi \mathbf{D} \cdot \nabla \omega) = q_\omega \tag{9}$$

where ω is mass fraction, q_ω is source term of mass transport and $\mathbf{D}$ is dispersion tensor following [27] with

$$\mathbf{D} = \tau D_m \boldsymbol{\delta} + \alpha_T |\mathbf{v}| \boldsymbol{\delta} + (\alpha_L - \alpha_T) \frac{v_i v_j}{|\mathbf{v}|} \tag{10}$$

where τ is tortuosity, D_m is coefficient of molecular diffusion, $\boldsymbol{\delta}$ is Kronecker-delta, α_T is transverse dispersivity and α_L is longitudinal dispersivity. Finally, (1) and (9) are iteratively coupled via the equation of bulk fluid density for an isothermal state, neglecting the compressibility of the fluid associated with the change of pressure described via

$$\rho(\omega) = \rho_0 (1 + \gamma_\omega \omega) \tag{11}$$

where ρ_0 is fluid density at $\omega = 0$, γ_ω is coefficient of expansion resulting from the change of mass fraction of the solute at constant pressure. The coefficient γ_ω for the relation between the densities of seawater and freshwater is given as $\gamma_\omega = 0.0245$ by Park and Aral [10] or as $\gamma_\omega = 0.026$ by Goswami and Clement [23] and depends on the mass of the dissolved ions.

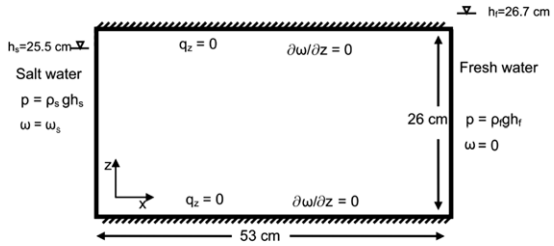

Fig. 1. Model domain and boundary conditions after [23] (altered, not to scale).

Table 1
Parameters of simulation.

Parameter	Setting
Porosity [–]	0.385
Permeability [m^2]	$1.239 \cdot 10^{-9}$
Residual reduction factor ζ_{res} [–]	0.0001
Residual reduction pressure p_{res} [Pa]	−100
Freshwater density ρ_f [kg m^{-3}]	1000
Saltwater density ρ_s [kg m^{-3}]	1026
Seawater–freshwater density relation γ_ω [–]	0.026
Longit./transv. dispersivity $\alpha_{L/T}$ [m]	$10^{-3}/10^{-4}$

3. Benchmark for density-dependent flow—the Goswami–Clement problem

3.1. Problem description

The Goswami–Clement problem shows density-dependent groundwater flow featuring a horizontally intruding saltwater from one side with higher density than the initially present freshwater and its displacement. This benchmark verifies the OGS model by comparing its simulation results with experimental and numerical Seawat simulation data [28] acquired by Goswami and Clement [23], who show a Henry-like [29] saltwater intrusion experiment using a laboratory-scale tank (Fig. 1).

3.2. Model setup

The boundary conditions are depicted in Fig. 1: *no-flow* boundaries are applied on bottom and top horizontal borders; vertical right and left hand side boundaries are described via linear pressure gradients $p_i(z = h_i) = \rho_i g h_i$, with $i = f$ for fresh water and $i = s$ for salt water, including the appropriate densities $\rho_f = 1000\ \mathrm{kg\,m^{-3}}$ or $\rho_s = 1026\ \mathrm{kg\,m^{-3}}$ and pressure heads $h_f = 0.267$ m and $h_s = 0.255$ m; the vertical right and left hand side boundary mass fraction ω represent fresh water (i.e. $\omega = 0$) and salt water (i.e. $\omega = 1$), respectively. Initial conditions are fresh water for the whole domain, i.e. a linear pressure gradient with $p(z = h_s = 0.255\ \mathrm{m}) = 0$ Pa and $\omega = 0$.

The domain consists of a homogeneous, isotropic material and resembles a medium coarse sand. The spatial dimensions of the laboratory tank were $0.53 \times 0.26 \times 0.027\ \mathrm{m^3}$ (length × height × width); a vertical 2D model domain was set up following the x-direction. The grid's discretization was uniform with rectangular quad-elements each of a size $\Delta x = \Delta z = 5 \cdot 10^{-3}$ m. The time step size was set to $\Delta t = 10$ s for a total simulation time of $t_{final} = 4800\ \mathrm{s} = 80$ min (time until steady state of experiment and simulation). Longitudinal dispersivity α_L was determined by laboratory experiments as $\alpha_L = 10^{-3}$ m, transversal dispersivity α_T was assumed to be $\alpha_T = 0.1 \cdot \alpha_L = 10^{-4}$ m. Diffusion effects can be neglected, if these are significantly smaller than mechanical dispersion:

$$\tau D_m \ll \alpha_T v. \tag{12}$$

Tortuosity is $\tau \approx 0.4$ [27], while diffusion coefficient is $D_m \approx 2.2 \cdot 10^{-9}\ \mathrm{m^2\,s^{-1}}$ [30]. The average fluid velocity is computed to $v \approx 40\ \mathrm{m} \cdot d^{-1}$; contributions of dispersion and diffusion can be compared via (12). It can be seen that diffusion effects are of minor importance in this study and can in fact be neglected. Further parameters are listed in Table 1.

3.3. Comparison of simulation results

The steady state of the experiment is shown in Fig. 2 depicting the OGS simulation results for mass fraction and the typical pattern of a saltwater intrusion front. The comparison of the experimental measurements with the modeling software outputs for Seawat and OGS are presented in Fig. 3 for mass fraction values of $\omega = 0.5$; the numerical results fit very well to the experimental observations. The slight deviations observed may be due to inhomogeneities of the sand material, or

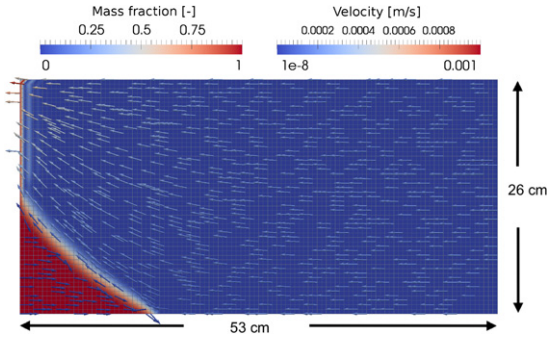

Fig. 2. Mass fraction, velocity vector flow field and grid resolution of the OGS steady-state simulation.

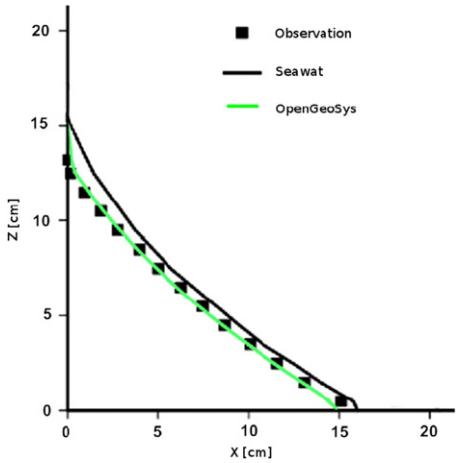

Fig. 3. Comparison of the $\omega = 0.5$ mass fraction isolines of experimental data with SEAWAT and OGS steady-state simulation, altered after [23].

Table 2
Simulation results: steady state right side boundary influx Q_{in} and deviation from experimental measurement σ.

Origin of value	Q_{in} [cm^3 s^{-1}]	σ [%]
Experiment	1.42	
SEAWAT	1.46	2.82
OGS	1.41	−0.70

due to the visual observation measurement technique used to obtain the isolines of $\omega = 0.5$. Goswami and Clement [23] describe the latter as follows: *"The color variations* [···] *indicate that the dispersion zone is relatively narrow and is estimated to be about* 1 cm *wide. Therefore the wedge delineation line* [···] *(which is assumed to be the* $\omega = 0.5$ *isoline) has an error in the range of* ±0.5 cm [···]". As the dispersion zone was estimated to be about 1 cm wide an in such a way *identified* $\omega = 0.5$ isoline could very well also depict the $\omega = 0.1$ or $\omega = 0.9$ isoline. From Fig. 2 it can be seen, that the dispersion zone width of the OGS simulation shows similar values as the experimental data of 1–1.5 cm. Further reading for the quantification of dispersion zone widths can be found in [31] or [32].

Additionally, the right boundary's inflow fluxes from measured experimental data, the SEAWAT results, and the equivalent values simulated with OGS are shown in Table 2. Again, both simulation outputs show only small deviation from the measured experimental data.

With the setup and parameters given by Goswami and Clement [23], the Peclet number can be determined after Eq. (13) to Pe = 50; although this is not perfectly in agreement with $2\alpha > \Delta x$, the code is still capable of showing results with little deviation from the experimental data.

$$\mathrm{Pe} = \frac{\Delta x}{\alpha}. \tag{13}$$

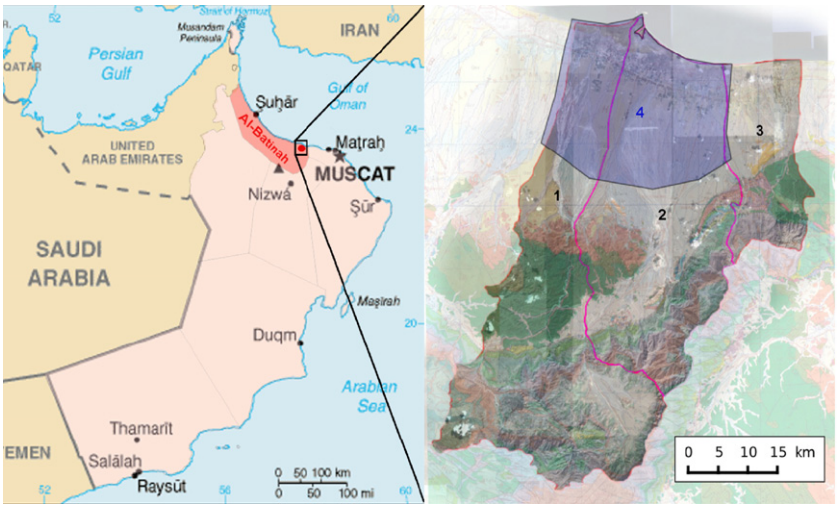

Fig. 4. Left: the Al-Batinah plain within Oman [33], altered; right: the three wadis (1 - Wadi Bani Kharus, 2 - Wadi Ma'awil, 3 - Wadi Taww) and the near coastal groundwater model domain (4).

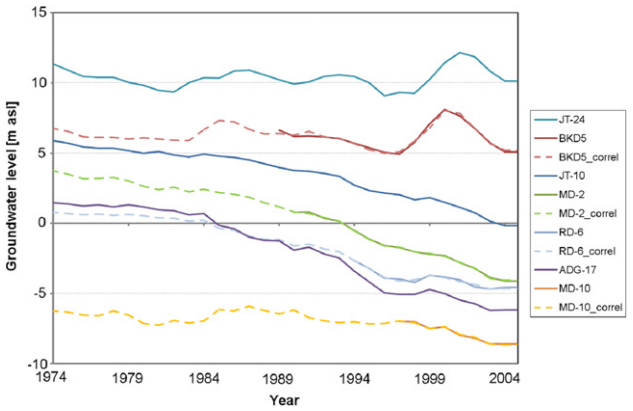

Fig. 5. Selection of groundwater level development data series for observation wells within the model area (solid lines) and correlation for incomplete data series (dashed lines, see Section 4.4).

4. Three-dimensional modeling in study area

In the following, we present the application of the validated numerical simulation software on a regional scale study area, calibration results of the heterogeneous three-dimensional groundwater model domain, and a scenario simulation.

4.1. The Al-Batinah study area

The Al-Batinah represents one of the major settlement areas in Oman (ca. 800,000 inhabitants) including both, large parts of different branches of industry and service providers, as well as tourism areas. Within the Al-Batinah, three catchments have been chosen for intensive studying: the wadis Ma'awil, Bani Kharus and Taww (Fig. 4).

Since soils are especially fertile in the coastal plains, most of the water is used for agricultural purposes (86%), followed by potable water (12%) and industrial usage (2%) [34]. Despite of a small proportion of water gained from desalinization, the substantial part is obtained from the local groundwater resources by a vast number of hand-dug and drilled wells. Estimations of various sources state increasing rates of abstraction from ca. $30 \cdot 10^6\ \mathrm{m}^3 \cdot a^{-1}$ in the 1970s, when pumping rates were assumed to be constant before, to a current abstraction rate of up to $120 \cdot 10^6\ \mathrm{m}^3 \cdot a^{-1}$ within the study region (compare [35,36]). The approximated inflow from the upstream mountainous areas yields only ca. $50 \cdot 10^6\ \mathrm{m}^3 \cdot a^{-1}$ [37]. The major impact of this considerably negative water balance of the coastal plain is the decrease of the groundwater table as observed since the late 1970s (Fig. 5). As a result, shallow wells of smaller farms and households run dry, forcing the people to abandon their homes and therewith endangering the traditional social structures and ways of living. Additionally, the decline of the water table causes the natural groundwater gradient to reverse. With the hydraulic gradient pointing inland,

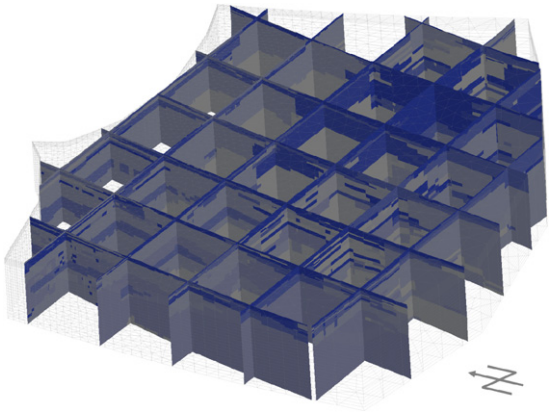

Fig. 6. Vertical cross sections of discrete interpolated hydrogeological aquifer types within groundwater model domain (compare area numbered 4 in Fig. 4), aquifer types from supposedly highly permeable gravelly (blue) to less permeable silty/clayey (white) sediments, with ten times vertical exaggeration. (For interpretation of the references to colour in this figure legend, the reader is referred to the web version of this article.)

seawater intrudes underneath the agricultural areas, limiting the availability of freshwater by a qualitative constraint (i.e. increase of salinity).

4.2. Data availability

For the development of possible scenarios, it is crucial to deal with proper real world data, especially for calibration purposes. However, data existence is sparse and the available data often lack completeness as well as consistence while containing few obviously wrong data due to systematic measurement errors. The latter were excluded from the data base. Available data are:

- Groundwater level measurements, roughly monthly for 1974–2005, only 15 of ca. 40 stations starting 1974, remaining series starting later
- Salinity measurements, temporal arbitrary measurements, no depth information
- Location of groundwater extraction sites, dug wells and borehole wells (compare Fig. 7(a) and (b))
- Total extraction estimates for 1970s and current time, temporal development of extraction rate increase until 2010
- Hydrogeological data, borehole logs and hydrogeological sections, data from pumping tests.

4.3. Hydrogeology and model domain

The hydrogeology of the study area exhibits a complex heterogeneous structure of fluviatile (esp. wadi), aeolian, and marine deposits, consisting of locally cemented gravels, differently sized sand, silt, loam and clay, as well as calcareous media opening a wide spectrum of possible hydrogeological parameter ranges. In the southern, mountainous areas, karstic structures are reckoned, that generally are subject to high modeling uncertainties [38]. Therefore the groundwater model domain starts where porous media deposits form mainly two aquifers (groundwater conducting formations): an upper, highly conductive and productive quaternary layer, and a lower, medium conductive tertiary layer. The aquifer structure is limited below by a clay layer with an extent that is subject to speculation in the near coastal zone due to missing observations (e.g. exploration boreholes, time-domain-electro-magnetic measurements). The total aquifer thickness increases from south to north shows a maximum of about 450 mbgl, while the quaternary aquifer has the largest thickness in the center of the model domain (the "Ma'awil trough") and thins out northwards [39]. The model domain extends over an area of ca. 30×25 km^2.

From the hydrogeological model, a three dimensional grid of 126,660 elements was built up using the Gmsh meshing software [40] forming a total of 30 layers. Grid resolution increases from the coastal area (min 150 m) to the south (max 2000 m). For the interpolation of the three-dimensional hydrogeological model, an adapted inverse weighted distance approach was used combining the available evaluated hydrogeological data from which a total of twelve individual material properties could be distinguished [41]. Fig. 6 shows several vertical cross sections through the study area. From the interpolation, the two above mentioned regional specialties can be identified: the Ma'awil trough, which serves as a highly conductive region for the throughflow of the groundwater recharge from the upstream mountainous area and the relatively thin quaternary aquifer in the coastal zone.

4.4. Conceptional model, parametrization and calibration techniques

The three basic components of the groundwater model's boundary conditions were: (i) the marine saltwater and level-zero-pressure boundary at the coast, (ii) the extraction from pumping activity, (iii) and the upstream subsurface inflow

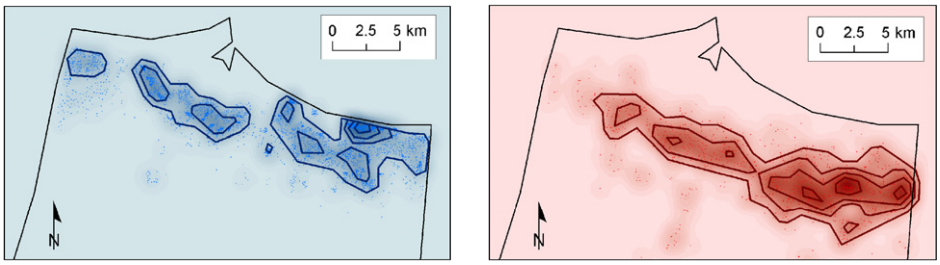

(a) Dug wells. (b) Drilled borehole wells.

Fig. 7. Kernel density distribution and simplified contour isoline polygons of the known extraction locations for drilled borehole and dug wells.

Table 3
Groundwater model domain simulation material parameters.

Parameter	Value
Porosity[a] ϕ [–]	0.02–0.385
Permeability (isotropic)[a],[b] k [m^2]	$1.239 \cdot 10^{-18}$–$1.239 \cdot 10^{-9}$
Residual reduction factor ζ_{res} [–]	0.0001
Residual reduction pressure p_{res} [Pa]	−1000
Longit./transv. dispersivity $\alpha_{L/T}$ [m]	200/20
Seawater–freshwater density relation γ_ω [–]	0.0245

[a] Parameter ranges given for the twelve hydrogeological materials.
[b] After calibration.

flux originating from the mountainous area's recharge from precipitation. Direct groundwater recharge from the wadi bed and recharge dam infiltration was not considered as their influence on the water balance is of minor importance [42].

The parametrization for (i) was a linear pressure head $p(z) = \rho_s g z$. For (ii), no information was available on the ca. 5000 wells' individual extraction rates; however, an overall estimation of the groundwater abstraction rate for the study area [36], the development of the pumping activity for the period 1974–2005, and the location of the single wells were known. While assuming an equal pumping rate per well type (dug well or borehole), the following procedure could incorporate the soft data of the known well locations into the numerical model: applying the overall specific abstraction rate (see Eq. (14)) on the simplified contour isoline polygons of a spatial kernel density filter [43], the uncertainties of the extraction boundary condition were reduced (see Fig. 7(a) and (b)). As an initial value for calibration, (iii) was based on an estimation of the mountainous recharge [37].

$$q_{\text{spec}} = \frac{Q_{\text{total}}}{\sum_{i=1}^{n} A_i} \tag{14}$$

where q_{spec} is specific abstraction rate, Q_{total} is total estimated abstraction rate by pumping activity and A_i is area of a simplified contour isoline polygon.

For the calibration of the model, the parametrization optimization software package PEST [44] was utilized. Basically, PEST uses the Marquardt-method to minimize a given target function (sum of weighted squared residuals) by varying a determined set of parameters until a critical threshold of the optimization criterion is reached. In this case, we used groundwater level measurements for the steady state calibration. PEST is a widely used parameter estimation tool [45–48]. The permeability of the twelve distinct materials and the boundary components (ii) and (iii) were subject to a steady state calibration for the pre-development phase before the 1970s. As no further information was available within the study area, permeability was treated isotropic. While running PEST, the calibration ranges of the 14 adjustable parameters were limited as percentage of their respective estimates from preliminary investigations as follows: permeability 0.1%–1000%, upstream inflow 5%–500%, aquifer extraction 10%–400%. It was taken care of, that the adjustable parameters do not exceed the stated parameter range boundaries.

Table 3 shows additional model parameters. Dispersivity is estimated from [49] and, again, diffusion was neglected following Eq. (12) with an average fluid velocity $v \approx 1\ \text{m} \cdot d^{-1}$.

As only 15 groundwater level measurements were available in the year 1974 from continuous time series (compare Section 4.2), a multiple linear correlation was used to gain supplemental calibration data. This was achieved by correlating each of the additional 25 time series starting later than 1974 to several continuous time series (see Fig. 5). The correlation periods are variable and depend on the individual beginning of the additional time series. Each correlation coefficient was $\rho'(x, y_1, \ldots, y_i) > 0.8$ with a mean of $\overline{\rho'(x, y_1, \ldots, y_i)} = 0.94$ resembling an acceptable correlation. The achieved supplemental data series were weighted by 0.1 within the target function of PEST.

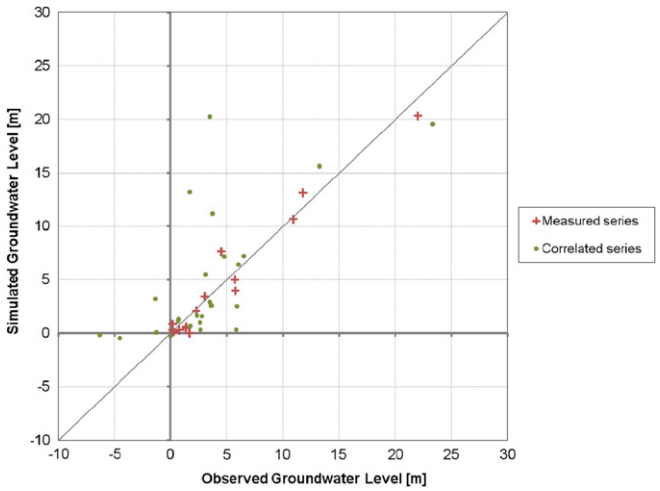

Fig. 8. Steady state 1974 scatter diagram for comparison of field data (red crosses are measured data, green circles are correlated data) and simulation output. (For interpretation of the references to colour in this figure legend, the reader is referred to the web version of this article.)

Table 4
Statistical parameters for the steady state 1974 calibration.

Statistical parameter	Value
Sum of squared weighted residuals [m^2]	29.610
Biased correlation coefficient [–]	0.979
Standard variance of weighted residuals [m^2]	1.184

4.5. Results steady state 1974 calibration and scenario simulation

Fig. 8 shows the scatter diagram for the steady-state calibration. The calibration result shows a good concordance between observed and simulated groundwater levels, especially for the 15 measured data points (red crosses). While the supplemental correlation originating data points (green circles) show a larger deviation than the measured data, these still have low residuals. Statistical parameters for the parameter optimization underline the good calibration, e.g. biased correlation coefficient >0.9 (see Table 4). PEST results for the hydrogeological materials (see Table 3), the upstream subsurface inflow $Q_{in,sub} = 6.80 \cdot 10^7\ m^3 \cdot a^{-1}$, and the abstraction $Q_{abstr,total} = 3.69 \cdot 10^7\ m^3 \cdot a^{-1}$ lie within the expected estimation ranges [36,37]. Fig. 9 shows the natural saltwater intrusion for the pre-development phase, i.e. pumping activity estimation for 1974 ($Q_{abstr,total}$). It can be recognized that the saltwater intrusion is relatively small, especially within the upper, highly permeable aquifer, as the upstream inflow is larger than abstraction and keeps the saline intrusion low. Also, within the highly heterogeneous flow field, the main discharge is routed through the center of the groundwater model domain, the "Ma'awil trough".

Using the steady state calibration results (Fig. 9 as the initial state) and the temporal estimation for the abstraction development since the 1970s, a transient scenario simulation was carried out. Fig. 10(a) and (b) compare results of the uncalibrated transient simulation and an interpolation of salinity measurements. Both figures generally depict similar patterns of the saltwater intrusion along the coast of the study area. Yet, the numerical results are not in perfect agreement with the measurements. This may be due to local phenomena that are not yet included in the setup, like the near-coastal Sabkha bay. Also, the current grid resolution of ≈200 m near the coast results in a too large Peclet number Pe ≈ 10 (see Eq. (13)), which shows potential for future optimization, when more precise salinity measurements are available for calibration.

5. Summary and outlook

We presented the extension of a Finite-Element-Model for non-linear coupled PDEs to simulate 3D density-dependent groundwater flow in an unconfined aquifer. The work shows the successful application of the open source scientific software package OGS solving the moving boundary problem for the numerical modeling of density-dependent groundwater simulations both in small and large scale domains.

The GOSWAMI–CLEMENT problem is solved to a sufficient degree in comparison to experimental data and SEAWAT simulation results. Although data availability is limited for the Oman study area, groundwater levels for a steady state could be calibrated. Additionally, the PEST calibration revealed good fitting to independent estimation studies of one of the calibration parameter (upstream inflow, [37]). Finally, scenario simulations depict saline intrusion patterns equivalent to

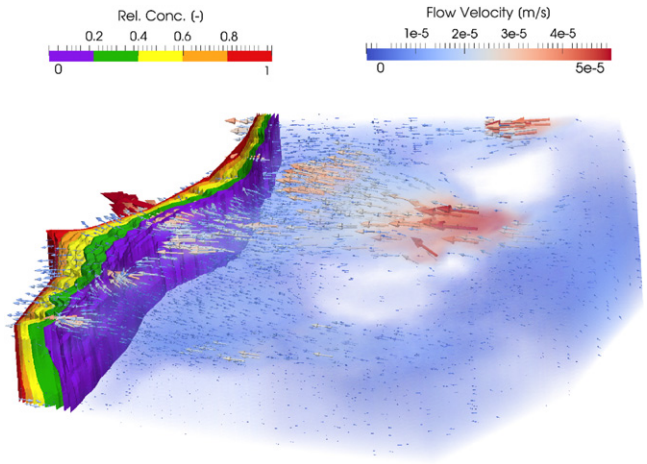

Fig. 9. Heterogeneous flow field in groundwater model domain, natural saltwater intrusion for steady state conditions, with ten times vertical exaggeration.

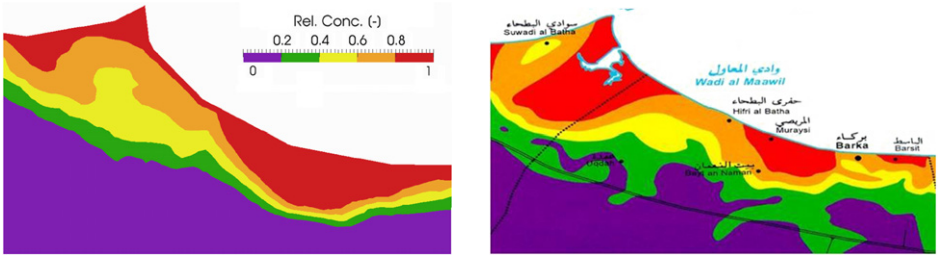

(a) Salinity simulation results.

(b) Salinity measurement interpolation.

Fig. 10. Comparison of results of transient mass transport scenario simulation and salinity measurement interpolation [50].

measurements and confirm the successful reproduction of the conceptual model, i.e. hydrogeological model and boundary conditions.

The 3D density-dependent groundwater model will be an important tool within an integrated water resources management system [51], which aims on a sustainable management of water quantity and quality of a coupled, dynamic agriculture–groundwater system. To support the existing scenario simulations, future works will include the calibration of transient flow and mass transport simulations. Depending on prospective available salinity measurement data, a depth-specific calibration for the mass transport model is possible. Other research reveals the potential of studying the sensitivity of the influence of anisotropy, dispersion, as well as spatial and temporal resolution on density-driven flow and mass transport in more detail on a regional scale [32,52]. Also, using an increased resolution of the groundwater model domain's grid, local density-dependent flow phenomena can be studied in more detail. Finally, the model will be coupled with groundwater recharge models of surface flow infiltration from the wadis and recharge dams of the study area (e.g. [53] or [54]) and a multiple target optimization method will be utilized for the optimization of possible future pumping sites' locations, their abstraction rates and the determination of a safe yield. Introducing advanced numerical methods into practical applications remains a challenging interdisciplinary field for both mathematicians and engineers.

Acknowledgments

This work is part of the International Water Research Alliance Saxony—IWAS joint research project and was funded by the German Federal Ministry of Education and Research (BMBF). The authors acknowledge the cooperation with the Omani Ministry of Regional Municipalities and Water Resources and appreciate the continuous exchange of data and knowledge.

References

[1] Y.Q. Xue, Y. Zhang, S.J. Ye, J.C. Wu, Q.F. Li, Land subsidence in China, Environmental Geology 48 (6) (2005) 713–720.
[2] P.M. Barlow, Ground Water in Freshwater–Saltwater Environments of the Atlantic Coast, Technical Report 1262, US Geological Survey Virginia, 2003.
[3] A. Cardona, J. Carrillo-Rivera, R. Huizar-lvarez, E. Graniel-Castro, Salinization in coastal aquifers of arid zones: an example from santo domingo, baja California sur, Mexico, Environmental Geology 45 (2004) 350–366.
[4] K.A. Narayan, C. Schleeberger, K.L. Bristow, Modelling seawater intrusion in the burdekin delta irrigation area, North Queensland, Australia, Agricultural Water Management 89 (3) (2007) 217–228.

[5] C.T. Simmons, Variable density groundwater flow: from current challenges to future possibilities, Hydrogeology Journal 13 (2005) 116–119.
[6] H. Abd-Elhamid, A. Javadi, A density-dependant finite element model for analysis of saltwater intrusion in coastal aquifers, Journal of Hydrology 401 (3–4) (2011) 259–271.
[7] T. Graf, L. Degener, Grid convergence of variable-density flow simulations in discretely-fractured porous media, Advances in Water Resources 34 (6) (2011) 760–769.
[8] A.D. Werner, J.D. Ward, L.K. Morgan, C.T. Simmons, N.I. Robinson, M.D. Teubner, Vulnerability indicators of sea water intrusion, Ground Water (2011) doi:10.1111/j.1745-6584.2011.00817.x.
[9] B. Datta, H. Vennalakanti, A. Dhar, Modeling and control of saltwater intrusion in a coastal aquifer of Andhra Pradesh, India, Journal of Hydro-environment Research 3 (3) (2009) 148–159.
[10] C.H. Park, M. Aral, Saltwater intrusion hydrodynamics in a tidal aquifer, ASCE Journal of Hydrologic Engineering 13 (9) (2008) 863–872.
[11] B.M. Giambastiani, M. Antonellini, G.H. Oude Essink, R.J. Stuurman, Saltwater intrusion in the unconfined coastal aquifer of ravenna Italy: a numerical model, Journal of Hydrology 340 (1–2) (2007) 91–104.
[12] A. Mazzia, M. Putti, Three-dimensional mixed finite element-finite volume approach for the solution of density-dependent flow in porous media, Journal of Computational and Applied Mathematics 185 (2) (2006) 347–359.
[13] M. Beinhorn, P. Dietrich, O. Kolditz, 3-D numerical evaluation of density effects on tracer tests, Journal of Contaminant Hydrology 81 (1–4) (2005) 89–105.
[14] A. Mazzia, M. Putti, Mixed-finite element and finite volume discretization for heavy brine simulations in groundwater, Journal of Computational and Applied Mathematics 147 (1) (2002) 191–213.
[15] H.J. Diersch, O. Kolditz, Variable-density flow and transport in porous media: approaches and challenges, Advances in Water Resources 25 (8–12) (2002) 899–944.
[16] C. Desai, Finite element residual schemes for unconfined flow, International Journal for Numerical Methods in Engineering 10 (1975) 1415–1418.
[17] C.S. Desai, G.C. Li, A residual flow procedure and application for free surface flow in porous media, Advances in Water Resources 6 (1983) 27–35.
[18] S. Sugio, C.S. Desai, Residual flow procedure for sea water intrusion in unconfined aquifers, International Journal for Numerical Methods in Engineering 24 (8) (1987) 1439–1450.
[19] M.M. Aral, Y. Tang, A new boundary element formulation for time-dependent confined and unconfined aquifer problems, Water Resources Research 24 (6) (1988) 831–842.
[20] T.R. MacDonald, P.K. Kitanidis, Modeling the free surface of an unconfined aquifer near a recirculation well, Groundwater 31 (5) (2005) 774–778.
[21] C. McElwee, M. Kemblowski, Theory and application of an approximate model of saltwater upconing in aquifers, Journal of Hydrology 115 (1990) 139–163.
[22] M. Meenal, T. Eldho, Simulation of groundwater flow in unconfined aquifer using meshfree point collocation method, Engineering Analysis with Boundary Elements 35 (4) (2011) 700–707.
[23] R.R. Goswami, T.P. Clement, Laboratory-scale investigation of saltwater intrusion dynamics, Water Resources Research 43 (2007).
[24] O. Kolditz, S. Bauer, L. Bilke, N. Böttcher, J. Delfs, T. Fischer, U. Görke, T. Kalbacher, G. Kosakowski, C. McDermott, C. Park, F. Radu, K. Rink, H. Shao, H. Shao, F. Sun, Y. Sun, A. Singh, J. Taron, M. Walther, W. Wang, N. Watanabe, Y. Wu, M. Xie, W. Xu, B. Zehner, OpenGeoSys: an open source initiative for numerical simulation of THMC processes in porous media, Environmental Earth Science (2012) doi:10.1007/s12665-012-1546-x.
[25] T. Kalbacher, J. Delfs, H. Shao, W. Wang, M. Walther, L. Samaniego, C. Schneider, A. Musolff, F. Centler, F. Sun, A. Hildebrandt, R. Liedl, D. Borchardt, P. Krebs, O. Kolditz, The IWAS-ToolBox: software coupling for an integrated water resources management, Environmental Earth Science 65 (5) (2011) 1367–1380. doi:10.1007/s12665-011-1270-y.
[26] J. Boussinesq, Recherches thoriques sur lcoulement des nappes deau infiltres dans le sol et sur le dbit des sources, Journal de Mathématiques Pures et Appliquées 5me Series 10 (1904) 5–78.
[27] J. Bear, Dynamics of fluids in porous media, in: Dover Books on Physics and Chemistry, Dover, 1988.
[28] Seawat. Homepage, 2011. http://water.usgs.gov/ogw/seawat/.
[29] H.R. Henry, Salt intrusion into coastal aquifers, Ph.D. Thesis, Columbia University, New York, USA, 1960.
[30] K. Tanaka, Self-diffusion coefficients of water in pure water and in aqueous solutions of several electrolytes with 18O and 2H as tracers, Journal of Chemical Society, Faraday Transactions 1 74 (1978) 1879–1881.
[31] L.J.T.M. Kempers, H. Haas, The dispersion zone between fluids with different density and viscosity in a heterogeneous porous medium, Journal of Fluid Mechanics 267 (1994) 299–324.
[32] J.L. Musuuza, F.A. Radu, S. Attinger, The effect of dispersion on the stability of density-driven flows in saturated homogeneous porous media, Advances in Water Resources 34 (3) (2011) 417–432.
[33] University of Texas Libraries, Small Map of Oman, 2010. http://www.lib.utexas.edu/maps/oman.html.
[34] S. Al-Shaqsi, The Socio-Economic and Cultural Aspects in the Implementation of Water Demand Management: A Case Study in The Sultanate of Oman, Master's thesis, University of Nottingham, 2004.
[35] Ministry of agriculture and fisheries. Bureau de Recherches Gologiques et Minires, Study of a New Organization of Irrigation in Barka–Rumais Area, Data Analysis and Modelling Report, Technical Report, 1992.
[36] S.S.M. Al-Shoukri, Mathematical Modeling of Groundwater Flow in Wadi Ma'awil Catchment, Barka in Sultanate of Oman. Master's thesis; Arabian Gulf University, Bahrain, 2008.
[37] A. Gerner, G. Schmitz, Portrayal of fuzzy recharge areas for water balance modelling—a case study in northern Oman, Advances in Geosciences (2011) accepted.
[38] M. Bakalowicz, Karst groundwater: a challenge for new resources, Hydrogeology Journal 13 (2005) 148–160. 10.1007/s10040-004-0402-9.
[39] P.G. Macumber, The cable tool program and groundwater flow in the eastern batinah alluvial aquifer, Technical Report, Ministry of Water Resources, Oman, 1998.
[40] C. Geuzaine, J.F. Remacle, Gmsh: a 3-D finite element mesh generator with built-in pre- and post-processing facilities, International Journal for Numerical Methods in Engineering 79 (11) (2009) 1309–1331.
[41] M. Walther, N. Böttcher, R. Liedl, A 3d interpolation algorithm for layered tilted geological formations using an adapted inverse distance weighting approach. in: Proceedings ModelCARE2011, IAHS Publ. 3XX, 201X. Leipzig, Germany, 2012 (in press).
[42] V. Eilers, R. Carter, K. Rushton, A single layer soil water balance model for estimating deep drainage potential recharge: an application to cropped land in semi-arid North–East nigeria, Geoderma 140 (1–2) (2007) 119–131.
[43] C. Brunsdon, Estimating probability surfaces for geographical point data: an adaptive kernel algorithm, Computers & Geosciences 21 (7) (1995) 877–894.
[44] J. Doherty, R. Hunt, Approaches to highly parameterized inversion—A guide to using PEST for groundwater-model calibration, Technical Report, US Geological Survey Scientific Investigations Report 2010–5169, 2010.
[45] M. Gallagher, J. Doherty, Parameter estimation and uncertainty analysis for a watershed model, Environmental Modelling & Software 22 (7) (2007) 1000–1020.
[46] F. El Yaouti, A. El Mandour, D. Khattach, O. Kaufmann, Modelling groundwater flow and advective contaminant transport in the Bou-Areg unconfined aquifer NE morocco, Journal of Hydro-environment Research 2 (3) (2008) 192–209.
[47] H. Li, P. Brunner, W. Kinzelbach, W. Li, X. Dong, Calibration of a groundwater model using pattern information from remote sensing data, Journal of Hydrology 377 (1–2) (2009) 120–130.
[48] F. Sun, H. Shao, T. Kalbacher, W. Wang, Z. Yang, Z. Huang, O. Kolditz, Groundwater drawdown at Nankou site of Beijing Plain: model development and calibration, Environmental Earth Sciences 64 (5) (2011) 1323–1333. 10.1007/s12665-011-0957-4.
[49] L.W. Gelhar, C. Welty, K.R. Rehfeldt, A critical review of data on field-scale dispersion in aquifers, Water Resources Research 28 (7) (1992) 1955–1974.

[50] Ministry of regional municipalities, environment and water resources, Water Resources in Oman, Technical Report, 2005.
[51] J. Grundmann, N. Schütze, G.H. Schmitz, S. Al-Shaqsi, Towards an integrated arid zone water management using simulation based optimisation, Environmental Earth Science (2012).
[52] J.L. Musuuza, F.A. Radu, S. Attinger, The stability of density-driven flows in saturated heterogeneous porous media, Advances in Water Resources 34 (11) (2011) 1464–1482.
[53] J. Delfs, C. Park, O. Kolditz, A sensitivity analysis of hortonian flow, Advances in Water Resources 32 (9) (2009) 1386–1395.
[54] A. Philipp, G. Schmitz, R. Liedl, An analytical model of surge flow in non-prismatic permeable channels and its application in arid regions, Journal of Hydraulic Engineering 136 (5) (2010) 290–298.